J. Fluid Mech. (2001), *vol.* 439, *pp.* 43–56. Printed in the United Kingdom

Gradient enhancement and filament ejection for a non-uniform elliptic vortex in two-dimensional turbulence

By Y. KIMURA[1,2] AND J. R. HERRING[2]

[1]Graduate School of Mathematics, Nagoya University, Furo-cho, Chikusa-ku, Nagoya 464-8602, Japan

[2]National Center for Atmospheric Research, P.O. Box 3000, Boulder, CO 80307, USA

(Received 5 December 1998 and in revised form 12 January 2001)

The axisymmetrization of a two-dimensional non-uniform elliptic vortex is studied in terms of the growth of palinstrophy, the squared vorticity gradient. First, it is pointed out that the equation for palinstrophy growth, if written in terms of the strain rate tensor, has a similar form to that of enstrophy growth in three-dimensions – the vortex-stretching equation. Then palinstrophy production is analysed, particularly for non-uniform elliptic vortices. It is shown analytically and verified numerically that a non-uniform elliptic vortex in general has a quadrupole structure for palinstrophy production, and that in the positive production regions, vortex filaments are ejected following the gradient enhancement process for vorticity. Numerical simulations are conducted for two different initial conditions, compact support and Gaussian vorticity distributions. These are characterized by distinctly different features of filament ejection and energy spectra. For both cases, the total palinstrophy production is a good indicator of the development of small-scale vorticity. In particular for the compact support case, a possible intermittency mechanism in the filament ejection process is proposed.

1. Introduction

Two-dimensional turbulence plays a vital role in our understanding of large-scale geophysical flows subject to rapid rotation and stable stratification. As with three-dimensional turbulence, the interplay of stretching and diffusion is the most essential physical mechanism in two-dimensional turbulence. The peculiarity of two-dimensional turbulence, however, stems from the fact that 'stretching' is not associated with vortex lines but with vorticity contours. In this paper, we shall consider this interplay and shed new light on it in relation to the gradient enhancement process, a vital nonlinear mechanism of two-dimensional fluid dynamics. The key ingredient on which our analysis focuses is the development of the square of vorticity gradient, the palinstrophy.

The isolated uniform elliptic vortex (the Kirchhoff vortex) continues to attract the attention of many vorticists, and indeed to play a fundamental and important role in the study of two-dimensional incompressible flow. The Kirchhoff vortex is a solution of Euler's equation consisting of a rotating ellipse of axes a and b with angular velocity $\Omega = \omega ab/(a+b)^2$, where ω is the uniform vorticity inside the ellipse. The stability of the Kirchhoff vortex was first presented for the linear case by Love (1893), who established that Kirchhoff's vortex with an aspect ratio greater than 3 is linearly

unstable. The stability analysis for Kirchhoff's vortex was later extended by Moore & Saffman (1971).

In contrast to Kirchhoff's vortex, the non-uniform elliptic vortex is not an exact solution of Euler's equation,† but still plays an important role in understanding the physics of gradient enhancement and vortex axisymmetrization, both of which are essential ingredients for the mechanism of large-scale vortex motion on the Earth, including hurricanes. As the pioneering work along this line, we can cite the work by Melander, McWilliams & Zabusky (1987) and subsequently by the group with Zabusky (Yao, Zabusky & Dritschel 1995; Dritschel & Zabusky 1996).

Melander *et al.* (1987) concluded that axisymmetrization of an elliptic vortex is effected by gradient enhancement of vorticity in the core and eventual ejection of a vorticity filament, pointing out that a non-uniform elliptic vortex is very unstable compared with Kirchhoff's vortex. The exact stability criterion as far as we know is, however, still an open problem.

We shall show that the above-mentioned mechanism, gradient enhancement and vorticity ejection, can be interpreted well in terms of the palinstrophy and its production. Also palinstrophy production can explain further the micro-mechanism which may bridge the two physical concepts in two-dimensional Navier–Stokes turbulence: gradient enhancement and vortex ejection. In particular, it will be shown both analytically and numerically that a non-uniform elliptic vortex in general has a quadrupole structure for the palinstrophy production, and that in the positive production regions, vortex filaments are ejected following the gradient enhancement process for vorticity. The decay of two-dimensional turbulence is, in general, characterized by a cascade of enstrophy (squared vorticity) to ever smaller scales. At sufficiently small scales, viscous dissipation balances the cascade, and the vorticity scale-size distribution declines faster than algebraically. The nonlinear aspects of this process conserve enstrophy, with spatial regions of strong cascade identified with positive production of palinstrophy. As the flow evolves, these 'cascade' regions comprise a progressively smaller fraction of the space available to the flow. Although the general aspects of the decay are deducible from statistical principles, the question of how intense are regions of palinstrophy production, and their spatial distribution has been entirely deduced from an examination of direct numerical simulations (DNS). The examination of vorticity patterns from such DNS frequently shows elliptical or circular vortex structures. Regions of strong palinstrophy production are seen to be spiral filamentary extrusions from regions of near elliptically organized vorticity. Hence palinstrophy production is a vital element in understanding of the dynamics of enstrophy cascade – particularly its extreme intermittent nature.

The paper is organized as follows. In § 2, we review the theory of the basic equation and palinstrophy production. Numerical results are then presented for two different sets of initial conditions corresponding to cut-off and Gaussian vorticity distributions in § 3, and the discussion and summary are given in § 4.

2. Theory

The vorticity equation in two dimensions is

$$\frac{\partial \omega}{\partial t} + (\boldsymbol{u} \cdot \nabla)\omega = \nu \nabla^2 \omega, \tag{2.1}$$

† Here by 'exact solution' we mean an isolated entity without changing its shape, which does not rule out the possibility of determining the functional form of evolution with respect to time and space.

where $\boldsymbol{u} = (u, v)$ is velocity and $\omega = \partial v/\partial x - \partial u/\partial y$ is vorticity and ν is kinematic viscosity. Introducing the stream function ψ as

$$u = \frac{\partial \psi}{\partial y}, \quad v = -\frac{\partial \psi}{\partial x}, \tag{2.2}$$

we can write the equations in the ω, ψ form as

$$\frac{\partial \omega}{\partial t} + J(\omega, \psi) = \nu \nabla^2, \tag{2.3}$$

where

$$J(\omega, \psi) = \frac{\partial \omega}{\partial x}\frac{\partial \psi}{\partial y} - \frac{\partial \omega}{\partial y}\frac{\partial \psi}{\partial x}$$

is the Jacobian.

Fom (2.3) we can obtain the following equation for the development of palinstrophy:

$$(\partial_t + \boldsymbol{u} \cdot \nabla)(\omega_x^2 + \omega_y^2) = 2\omega_x\omega_y(\psi_{xx} - \psi_{yy}) + 2\psi_{xy}(\omega_y^2 - \omega_x^2) + 2\nu(\omega_x(\nabla^2\omega)_x + \omega_y(\nabla^2\omega)_y) \tag{2.4}$$

where a subscript means the derivative in that direction. Making use of the rate of strain tensor,

$$\boldsymbol{S} = \begin{pmatrix} u_x & \frac{1}{2}(u_y + v_x) \\ \frac{1}{2}(u_y + v_x) & v_y \end{pmatrix} = \begin{pmatrix} \psi_{xy} & \frac{1}{2}(\psi_{yy} - \psi_{xx}) \\ \frac{1}{2}(\psi_{yy} - \psi_{xx}) & -\psi_{xy} \end{pmatrix},$$

equation (2.4) can be rewritten as

$$\frac{\mathrm{D}|\nabla\omega|^2}{\mathrm{D}t} = \underbrace{-2\frac{\partial \omega}{\partial x_i}\frac{\partial \omega}{\partial x_j}S_{ij}}_{P_s} + \underbrace{2\nu\frac{\partial \omega}{\partial x_i}\frac{\partial(\nabla^2\omega)}{\partial x_i}}_{P_d}. \tag{2.5}$$

Batchelor (1969) has presented the formula for the volume average of (2.5).

It is notable that for three-dimensional turbulence an analogous relation holds for the square of vorticity called enstrophy, namely (Batchelor 1967, p. 277)

$$\frac{\mathrm{D}|\boldsymbol{\omega}|^2}{\mathrm{D}t} = 2\,\omega_i\omega_j S_{ij} + 2\nu\omega_i\nabla^2\omega_i, \tag{2.6}$$

where ω is the magnitude of the vorticity vector, and S_{ij} is the rate of strain tensor in three dimensions. After neglecting the viscous term (and hereafter we will concentrate only on the nonlinear term), equation (2.6) provides all the basics for the analysis of vortex stretching in three-dimensional turbulence. For a summary of research on this topic, see Tsinober, Shtilman & Vaisburd (1997). The importance of (2.5) as well as (2.6) is that the Lagrangian dynamics of the magnitude of vorticity and vorticity gradient is described by the components of these quantities and the field data in an Eulerian way. The sign of coefficients or the growth rates of the magnitude if we regard the equations as a self-induction which is deformed by the strain, however, differ in (2.5) and (2.6). The effect of this difference is yet to be known.

To gain some insight into the dynamics of the development of an elliptic vortex in general, we assume that the stream function ψ is of the form, $\psi(x, y) = F(ax^2 + by^2)$, where F is an arbitrary (differentiable) function, and calculate the functional form of

P_s. Direct substitution gives

$$\begin{aligned} P_s &= 64\,ab(a-b)\,xy \\ &\quad \times[-4(F'')^2\{(3a^3x^2+a^2bx^2+ab^2y^2+3b^3y^2)F''+2(a^2x^2+b^2y^2)^2F''''\} \\ &\quad +F'\{(3a^2+10ab+3b^2)(F'')^2+8(a+b)(a^2x^2+b^2y^2)F''F''' \\ &\quad +4(a^2x^2+b^2y^2)^2(F''')^2\}] \\ &\equiv ab(a-b)\;xy\;G(x^2,y^2,a,b), \end{aligned} \tag{2.7}$$

where a prime denotes differentiation with respect to $z = ax^2 + by^2$, and G is a functional of F.

From the above, we can observe that:

(i) $P_s = 0$ for a circular vortex ($a = b$),

(ii) the x- and y-axes are boundaries which separate the regions of the positive and negative palinstrophy production, and discounting a dominant effect from $G(x^2, y^2, a, b)$, P_s has a quadrupole structure (cf. § 4), and

(iii) if we assume that $ab(a-b)$ has a dominant contribution, under conditions of $a+b=1$ and $a>b$, P_s takes the maximum value at $a = \frac{1}{6}(3+\sqrt{3})$.

We should note that a non-zero P_s distribution in an isolated vortex does not necessarily mean that the vortex is unsteady. In fact, the Lamb–Batchelor dipole vortex has a symmetric distribution of positive and negative P_s inside, though it is a steady solution of Euler's equation and propagates without changing its shape. In this case, there should be a subtle balance between enhancement and suppression of vorticity gradient with the steady propagation of the vortex. On the other hand, in two-dimensional turbulence, the normalized volume average of P_s (the two-dimensional skewness) measures the strength of the cascade of enstrophy to small scales (see e.g. Herring *et al.* 1974).

3. Numerical simulation

As the initial vorticity fields, we use two different sets of smooth distributions. One is a compact support and the other is a Gaussian distribution. Both have concentric elliptic equivorticity lines. The assumption of concentric elliptic distribution of vorticity gives a slightly different testing ground from that for concentric elliptic stream functions which we assumed in the last section. In fact, the former provides a similar but non-concentric elliptic stream function which tends to be more and more circular as the distance from the origin increases. The following numerical simulations will examine some of the predictions made in the last section, and we shall see that the concentric elliptic vortices do have the quadrapole structure for P_s.

To integrate the Navier–Stokes equation, the pseudo-spectral method is used with 2048^2 grid points and dealiasing by the 2/3-rule. The time marching scheme is a third-order Runge–Kutta method with a fixed time step.

3.1. *Compact support*

As the initial distribution of vorticity we adopt the one used by Melander *et al.* (1987),

$$\omega(r) = \omega_0\left[1-\exp\left\{-C\frac{R_0}{r}\exp\left(-\frac{R_0}{R_0-r}\right)\right\}\right] \quad (0 \leqslant r < R_0) \tag{3.1}$$

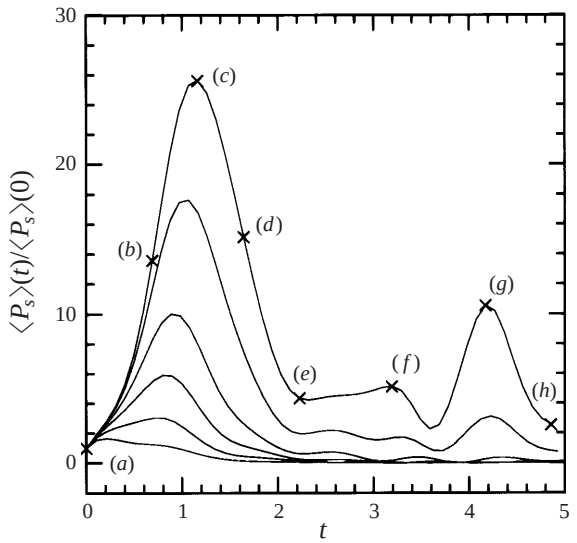

FIGURE 1. The growth of the volume average of the palinstrophy production P_s in (2.5) for various initial microscale Reynolds numbers in the compact support case. ($R_\lambda(0) = 2398, 1199, 480, 240, 120, 60$ from the top to the bottom.) The values are normalized by the initial value.

where $r = \sqrt{ax^2 + by^2}$, and $\omega(r)$ satisfies $\omega(r \to 0) \to \omega_0$, $\omega(r \to R_0) \to 0$, and we chose $C = 2.5608517$ so that $\omega(R_0/2) \sim \omega_0/2$, and the cut-off radius $R_0 = \pi/2$. As the initial shape of the ellipse we used $(a, b) = (10, 1)$ which gives the aspect ratio $\sqrt{10} > 3$, which is in the unstable regime in terms of the linear stability for Kirchhoff's vortex. Figure 1 is the growth of the volume average of P_s normalized by the initial value for different initial Reynolds numbers. We see that:

(i) the initial peak becomes higher for larger Reynolds numbers,

(ii) the curves are oscillatory for all the time range calculated, and the amplitude grows with Reynolds number, and

(iii) a secondary peak develops for larger Reynolds numbers.

To see the behaviour of the ellipse, we show sequential snapshots of equivorticity contour lines with the value of P_s in (2.5) in figure 2. The sequence is along the curve for the largest Reynolds number in figure 1 and the times and values of the total P_s are specified by the cross marks on the curve. In figure 2, the colour code is normalized by a hyperbolic tangent function so that structures with smaller values of P_s can be seen.

At $t = 0$ the ellipse is located with the longer axis vertical, which has the quadrupole structure in terms of the palinstrophy production with the x- and y-axes as boundaries just as predicted by the theory in § 2 (figure 2*a*). In the figure, the first and third quadrants have negative values of P_s while the second and fourth quadrants have positive values.

As the ellipse rotates anti-clockwise, the contour lines inside get closer in the positive quadrants. At the same time the regions are stretched and begin to eject vortex filaments, while the negative quadrants are pushed concentrically and contracted (figure 2*b*) (equivalent observations were reported in Melander *et al.* (1987) though they did not use the palinstrophy production and the quadrupole structure of it for their analysis). It is seen that the outer edge of the spirals has a significant positive P_s value.

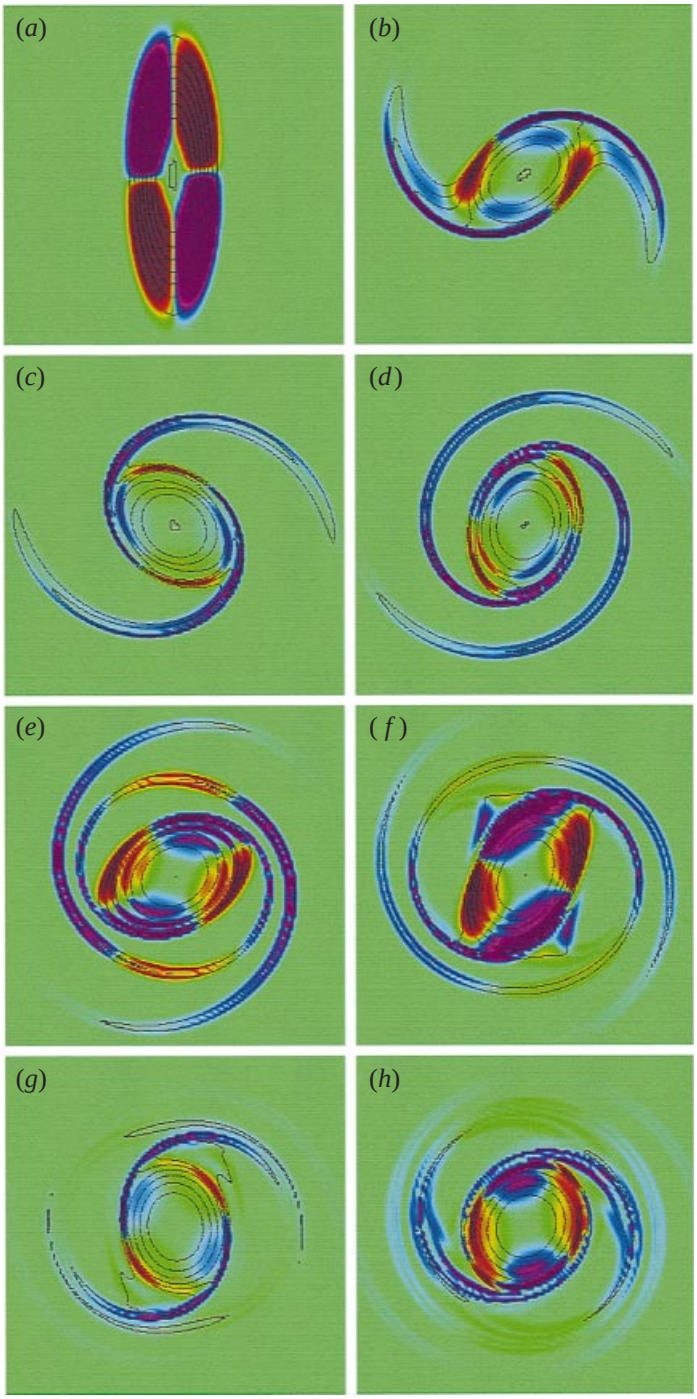

FIGURE 2. Snapshots of the equivorticity contour lines, with colour indicating the value of the palinstrophy production for compact support initial conditions. The data are sampled for the highest $R_\lambda(0)$ case, and the sampling times are indicated by the cross marks with corresponding labels on the plot in figure 1.

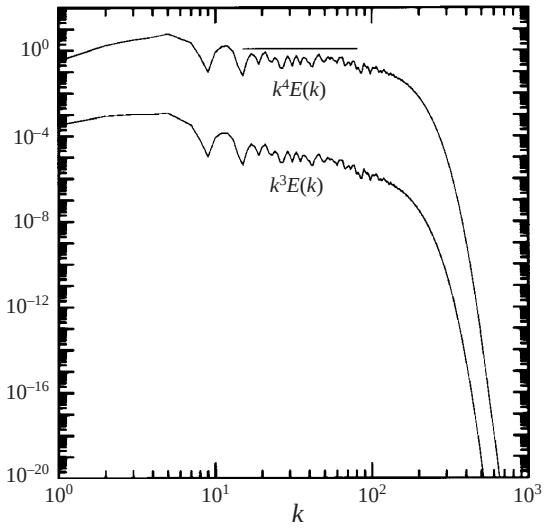

FIGURE 3. The compensated energy spectra, $k^4E(k)$ and $k^3E(k)$, for the compact support case at $t = 4.76$. The latter is shifted down by 3 decades.

The filaments continue to grow, and at the time of figure 2(*c*) the total P_s takes the maximum value and the situation corresponds to the case of the most stretched filaments outside the vortex core; we see only small negative P_s regions mainly concentrated at the edges of the core.

While the core region rotates and becomes surrounded by the filaments, the negative P_s regions grow inside (figure 2*d*). Then even in the filaments the negative P_s regions appear (figure 2*e*, *f*), and eventually the filaments disconnect from the core region (figure 2*g*). Figure 2(*g*) corresponds to the secondary peak of the total P_S in figure 1, and a similarity with the state in figure 2(*c*) can be observed except for the disconnected filaments and the slight change in the core boundary. It seems that the vortex filament ejection for this initial distribution repeats and thus it is in a sense intermittent, and the intermittency can be verified with the plot of total P_s.

Figure 3 is the energy spectrum at $t = 4.76$ (close to the time of figure 2*h*). It is compensated by the factor k^4 and k^3 for comparison. (The latter is shifted down by 3 decades.) These factors k^4 and k^3 are from the two distinctive theories on the inertial-range spectrum for two-dimensional turbulence; the former by Saffman (1971) which is based on discontinuity of vorticity in the shearing motion of fluids, and the latter by Kraichnan (1967) (with a logarithmic correction) and Batchelor (1969) which assumes an enstrophy cascade. The one with the factor k^4 almost levels, with fluctuations, in particular in the middle range of the wavenumber, $20 < k < 70$.

Figure 4 shows the average of palinstrophy production $P(P_s|\omega)$ conditionally sampled from the set of equal magnitude of vorticity at the times of figures 2(*a*) to 2(*g*) (i.e. at the marked positions in figure 1). The figure is plotted as a function of the magnitude of vorticity, and the values are normalized by the maximum value. We observe that the palinstrophy production stays almost zero at zero vorticity (background) and at the maximum vorticity (core). The core has effectively no palinstrophy production because of cancellation, even though the core contains both strong positive and negative regions.

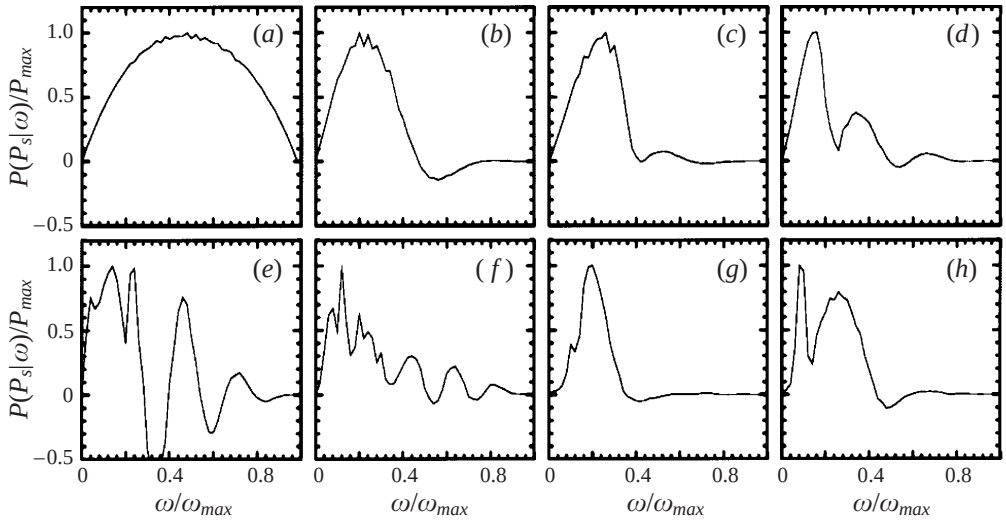

FIGURE 4. Conditional average of the palinstrophy production in terms of the magnitude of vorticity for the compact support case. The labels correspond to those in figure 1 and figure 2.

At $t = 0$, the shape of the conditional average is symmetric and the peak is at the middle value of vorticity (figure 4*a*). Until the first peak appears in figure 1, the peak shifts to the left (figure 4*b*, *c*). The shift of the peak to the smaller vorticity means that the main contribution to the palinstrophy production comes from the scattered weak vorticity filaments. After passing the first peak in figure 1, the conditional average shows rather violent oscillations, but with the major peak being still in the low vorticity region (figure 4*d–f*). The oscillation disappears by the time of the second peak in figure 1 (figure 4*g*). Again after passing the second peak, we can observe oscillations, in particular in the lower vorticity region. This conditional average of P_s enables us to verify the intermittency of vortex filament ejection.

3.2. *Gaussian distribution*

As the second type of vorticity distribution, we use the Gaussian distribution

$$\omega(r) = \omega_0 \exp\{-Cr^2\} \quad (0 \leqslant r < R_0) \tag{3.2}$$

where $r = \sqrt{ax^2 + by^2}$ and we chose $C = 2.8092\ldots$ so that $\omega(R_0/\sqrt{10}) \sim \omega_0/2$. In this case, the initial microscale Reynolds number is similar to the compact support case. The radius is also $R_0 = \pi/2$. We look at the development of the ellipse in terms of the same issues as before.

Figure 5 is the growth of the volume average of P_s normalized by the initial value for different initial Reynolds numbers. We see that:

(i) the initial peak becomes higher for larger Reynolds numbers as before,

(ii) the curves show no oscillation after the peak even for higher Reynolds numbers, and eventually

(iii) there is no secondary peak.

Figure 6 is sequential snapshots of equivorticity contour lines coloured with the value of P_s. (The sampling times of the snapshots are marked on the curve for the largest Reynolds number in figure 5.)

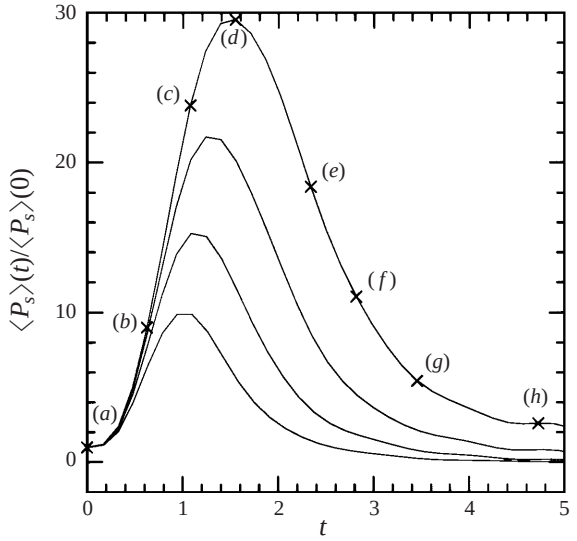

FIGURE 5. The growth of the volume average of the palinstrophy production for various initial microscale Reynolds numbers for the Gaussian case. ($R_\lambda(0) = 2338, 1169, 585, 292$ from the top to the bottom.) The values are normalized by the initial value.

At $t = 0$ the ellipse is located with the longer axis vertical. Even though the initial stage of the development is similar to the compact case (figure 6*a*, *b*), clearly we can observe that (i) the filament is less stretched and (ii) the core is more circular than the compact support case (figure 6*c*). The circular core persists for a long time and the filament winds around it quite continuously in space and time (figure 6*d*–*g*). In figure 6(*h*), however, some defects of the spirals are seen at the root in the core region. Disconnection of the filaments is observed at the root at the edge of the core where P_s takes negative values.

Figure 7 is the energy spectrum at $t = 4.73$ (*a*) (the time corresponds to that for figure 6*h*), and at $t = 7.77$ (*b*). Plots of $k^3E(k)$ together with $k^{11/3}E(k)$ and $k^4E(k)$ are presented for comparison. At the earlier time levelling of the k^3 compensated spectrum is observed, with fluctuations in the middle range of the wavenumber, around $20 < k < 60$. At the later time, however, a normalization $k^{11/3}E(k)$ by Gilbert (1988) and Moffatt (1990) which is based on the existence of spiral structures seems to work better.

Similarly to figure 4, figure 8 shows the average of palinstrophy production $P(P_s|\omega)$ conditionally sampled from the equal magnitude set of vorticity at the times corresponding to figure 6(*a*–*g*) (i.e. at the marked positions in figure 5).

Again we see that the palinstrophy production stays almost zero at zero vorticity (background) and at the maximum vorticity (in the core). Also the main peak shifts to the smaller vorticity. Unlike the previous case, however, the average shows clear oscillation (figure 8*e*–*h*). It is almost certain that the oscillation is due to the spirals. The amplitude of the oscillation decreases except for the main peak (figure 8*h*) and we expect that only the main peak survives asymptotically as time goes on. The contrast seems interesting between the oscillatory behaviour in space and the rather smooth development of the total palinstrophy in time.

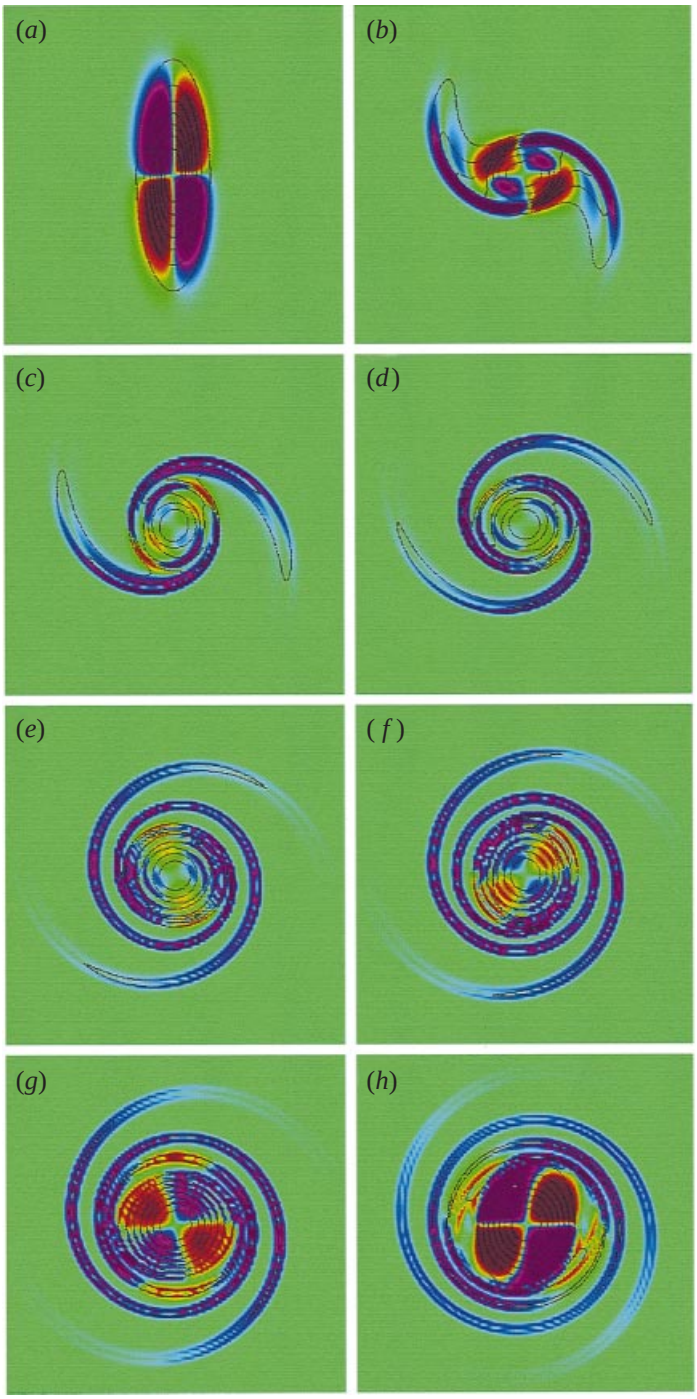

FIGURE 6. Snapshots of the equivorticity contour lines with colour indicating the value of the palinstrophy production for Gaussian initial conditions. The data are sampled for the highest $R_\lambda(0)$ case, and the sampling times are indicated by the cross marks with the labels on the plot in figure 5.

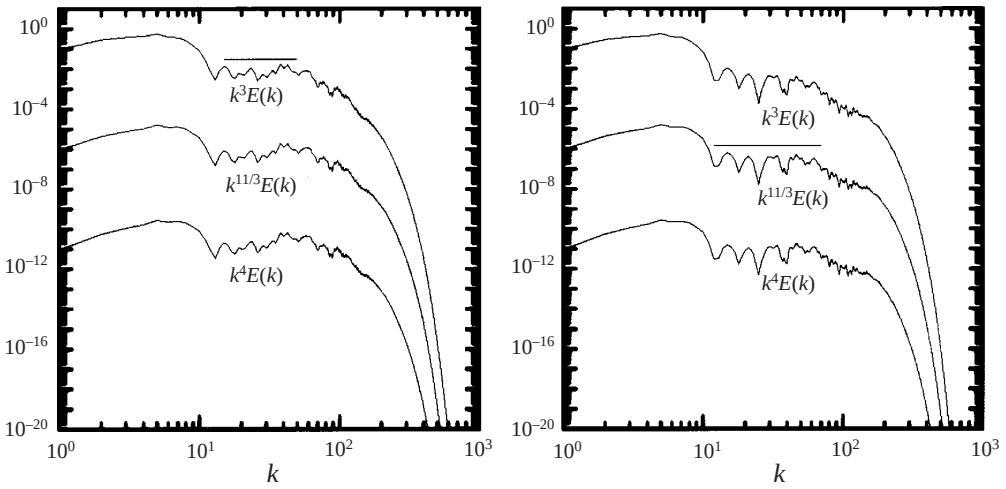

FIGURE 7. The compensated energy spectrum, $k^3E(k)$, $k^{11/3}E(k)$ and $k^4E(k)$, for the Gaussian initial condition (*a*) $t = 4.73$ and (*b*) $t = 7.77$. The last two are shifted down by 5 decades each.

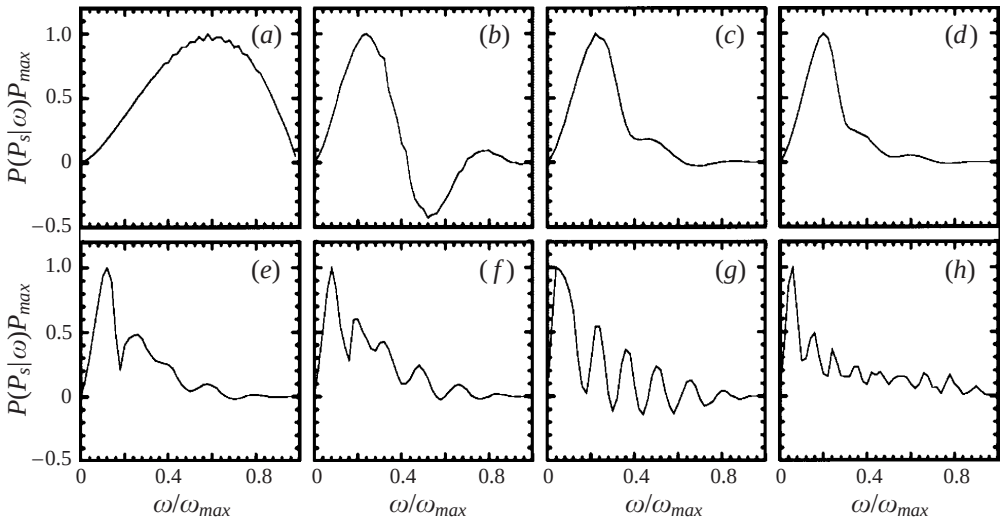

FIGURE 8. Conditional average of the palinstrophy production in terms of the magnitude of vorticity for the Gaussian case. The labels correspond to those in figure 5 and figure 6.

4. Discussion

Figure 9 shows a snapshot of vorticity contours (black: positive; red: negative) from the pseudo-spectral simulation with a random Gaussian initial condition which is coloured as before by the value of the palinstrophy production. The domain shown is the one-eighth centre-cut of the total domain of 2048^2 grid points.

We see a number of elliptic vortices which have a quadrupole structure of the palinstrophy production just as the single elliptic vortex in the preceding section. The abundance of non-uniform elliptic vortices which carry very similar quadrupole structure to a single elliptic vortex suggest the applicability of the present simplified theory to more general situations including turbulence.

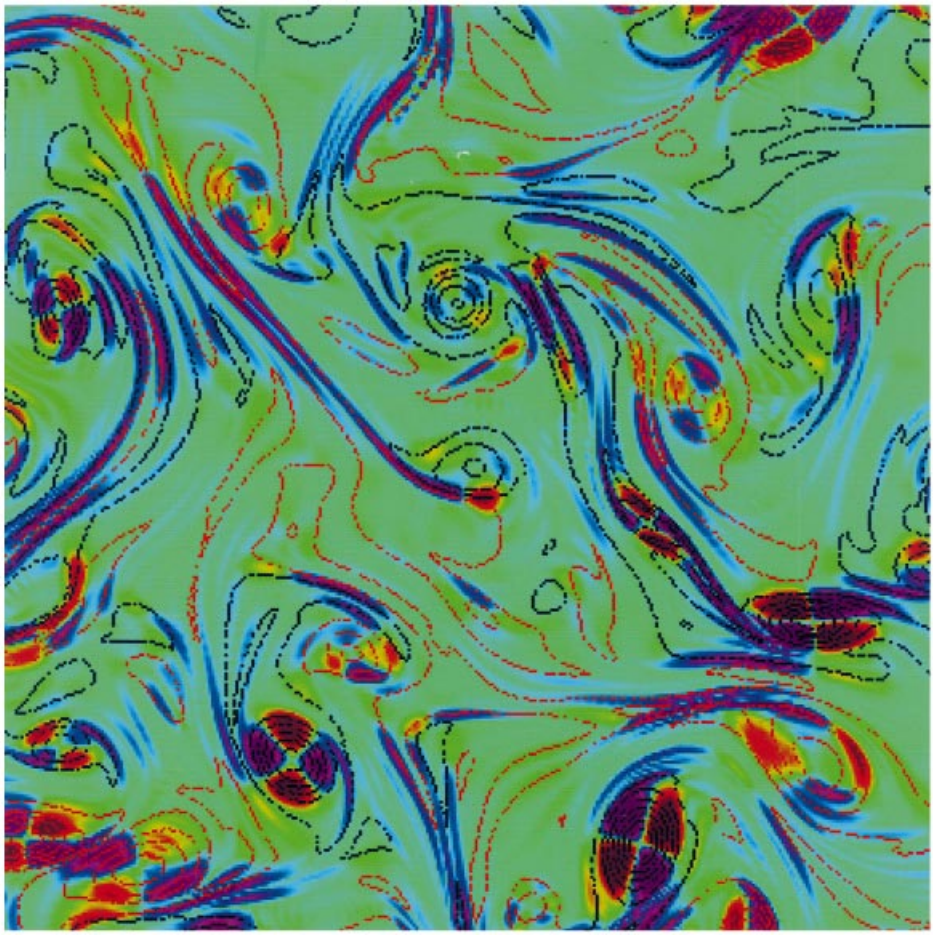

FIGURE 9. Snapshot of vorticity contours (black: positive; red: negative) colored by the value of the palinstrophy production from the pseudo-spectral simulation with a random Gaussian initial condition.

One of the major differences for the random case is that the filaments ejected from elliptic vortices sometimes maintain strong palinstrophy production as well as vorticity due to the nonlinear interaction from other vortices and filaments in the background flow.

It is interesting to note that a non-uniform elliptic vortex in general has the quadrapole structure for palinstrophy production, P_s, and that the second and fourth quadrants in a (positive) elliptic vortex are fated to undergo positive stretching even without any effect of outer flows. Here we would like to repeat and summarize the scenario of the vorticity gradient enhancement and subsequent filament ejection. First, vorticity gradient enhancement by positive palinstrophy production results in overtaking of contour lines, which is reminiscent of the front (or the singularity) genesis in fluids. Owing to incompressibility, the squashing of the region is compensated by ejecting and stretching a vorticity filament from the tip. The direction of stretching is determined as perpendicular to the maximum vorticity gradient.

The near final stage of two-dimensional turbulence in a bounded domain is an interesting subject. From a previous study, the final stage may be a vortex lattice with only one vortex in each fundamental cell (Matthaeus *et al.* 1990). From the view point of palinstrophy production, a circular (or axisymmetric) vortex produces no palinstrophy, and is qualified as a steady-state solution of the two-dimensional Navier–Stokes equations. Perhaps shielding by the cloud of (weak) palinstrophy production maintains the circular shape of a vortex even in the earlier stage of development.†

It is still an open question how much can be deduced about the statistics of two-dimensional turbulence in terms of the present theory on palinstrophy production. One way forward we can propose is (as we did in § 2) to develop the stretching analysis in two-dimensional turbulence and compare with three-dimensional turbulence. The governing equation for stretching in two-dimensions (2.5) has a similar form in three-dimensions (2.6), but with the obvious difference that the former has an opposite sign for the production term to the latter. The essential difference in the stretching due to this sign difference should be studied in the future. In any event, however, we can say and have verified that the non-uniform elliptic vortex is the simplest non-trivial building block found yet to construct the theory which elucidates the stretching mechanism in two-dimensional turbulence.

The authors are grateful to Arkady Tsinober and Rich Rotunno for valuable suggestions and encouragement, and Norman Zabusky for providing his reprints on two-dimensional turbulence. Y. K. acknowledges the support by a Grant-in-Aid (08404006) for Scientific Research from the Ministry of Education, Science, and Culture of Japan. NCAR is sponsored by the National Science Foundation.

REFERENCES

Batchelor G. K. 1967 *An Introduction to Fluid Dynamics*. Cambridge University Press.

Batchelor G. K. 1969 Computation of the energy spectrum in homogeneous two-dimensional turbulence. *Phys. Fluids supplement II*, 233–239.

Dritschel, D. G. 1998 On the persistence of non-axisymmetric vortices in inviscid two-dimensional flows. *J. Fluid Mech.* **371**, 141–155.

Dritschel, D. G. & Zabusky, N. J. 1996 On the nature of vortex interactions and models in unforced nearly-inviscid two-dimensional turbulence. *Phys. Fluids* **8**, 1252–1256.

Gilbert, A. D. 1988 Spiral structures and spectra in two-dimensional turbulence. *J. Fluid Mech.* **193**, 475–497.

Herring, J. R., Orszag, S. A., Kraichnan, R. H. & Fox, D. G. 1974 Decay of two-dimensional homogeneous turbulence. *J. Fluid Mech.* **66**, 417–444.

Kraichnan, R. H. 1967 Inertial ranges in two-dimensional turbulence. *Phys. Fluids* **10**, 1417–1423.

Love, A. E. H. 1893 On the stability of certain vortex motions. *Proc. Lond. Math. Soc.* **25**, 18–42.

Matthaeus W. H., Stribling, W. T., Martinez, D., Oughton, S. & Montgomery, D. 1991 Selective decay and coherent vortices in two dimensional incompressible turbulence. *Phys. Rev. Lett.* **66**, 2731–2734.

Melander, M. V., McWilliams, J. C. & Zabusky, N. J. 1987 Axisymmetrization and vorticity-gradient intensification of an isolated two-dimensional vortex through filamentation. *J. Fluid Mech.* **178**, 137–159.

Moffatt, H. K. 1990 Spiral structures in turbulent flows. Preprint of the lecture at the IMA Conference on 'Wavelets, Fractals, and Fourier Transforms: New Developments and New Applications', Cambridge, UK, 17–18 December (unpublished).

† Recently, Dritschel (1998) pointed out a possibility of a steady non-axisymmetric vortex. The existence of such solutions may be examined by the concept reported in this paper.

Moore, D. W. & Saffman, P. G. 1971 Structure of a line vortex in an imposed strain. In *Aircraft Wake Turbulence* (ed. J. H. Olsen, A. Goldburg, & M. Rogers), pp. 339–354. Plenum.

Saffman, P. G. 1971 On the spectrum and decay of random two-dimensional vorticity distributions at large Reynolds number. *Stud. Appl. Maths* **50**, 377.

Saffman, P. G. 1992 *Vortex Dynamic*. Cambridge University Press.

Tsinober, A., Shtilman, L. & Vaisburd, H. 1997 A study of properties of vortex stretching and enstrophy generation in numerical and laboratory turbulence. *Fluid Dyn. Res.* **21**, 477–494.

Yao, H. B., Zabusky, N. J. & Dritschel, D. G. 1995 High gradient phenomena in two-dimensional vortex interactions. *Phys. Fluids* **7**, 539–548.